A new one point quadrature rule over arbitrary star convex polygon/polyhedron

S. Natarajan[a], A. Francis[a], E. Atroschenko[b]
S. P. A. Bordas[c,d,e]

Abstract The Linear Smoothing (LS) scheme [1] meliorate the linear and quadratic approximations over convex polytopes by employing three-point integration scheme. In this work, we propose a linearly consistent one point integration scheme which possesses the properties of the LS with three point integration scheme. The core essence of the proposed technique is to approximate the strain by the smoothed nodal derivatives that are determined by the discrete form of the divergence theorem. This is viable by Taylor's expansion of the weak form which facilitate the evaluation of the smoothed nodal derivatives acting as the stabilization terms. The orthogonality condition between the compatible and the smoothed nodal derivatives at the point of integration is satisfied with the Taylor's expansion technique. The smoothed nodal derivatives are evaluated only at the centroid of each integration cell. These integration cells are the simplicial subcells (triangle/tetrahedron in two & three dimensions) obtained by subdividing the polytopes. The smoothed nodal derivatives evaluated at the centroid of each subcell is used to compute the smoothed stiffness matrix. The convergence properties, the accuracy, and the efficacy of the LS with one point integration scheme, especially its superiority over the LS with three point integration scheme are discussed by solving few benchmark problems.

Keywords Polygonal finite element method, Wachspress shape functions, numerical integration, linear consistency, one point integration.

1 Introduction

The Finite Element Method (FEM) is one of the most efficient and robust numerical methods preferred to solve various complex engineering problems. The conventional FEM uses triangular and quadrilateral elements in two dimensions to discretize the domain. The development of finite elements on arbitrary polytopes coined as the Polygonal Finite Element Method (PFEM) in engineering problems came into existence very recently [2],[3], [4],[5]. The polygonal elements are more preferable over the conventional finite elements in many aspects like the flexibility in meshing complex geometries with the help of various meshing algorithms developed based on the concept of Voronoi tessellation [5], modeling of complex geometries with inclusions [6], modeling of polycrystalline materials [7], [8]. Furthermore, polygonal/polyhedral elements are also useful to solve problems on large deformation [9], [10], incompressibility [11], contact problems [12] and fracture mechanics [13]. The polygonal finite elements also simplifies the procedures of adaptive mesh such as local refinement and coarsening since their is no problem of hanging nodes [14]. Different methods are available using arbitrary polytopes [15] of which some of these techniques are: Mimetic Finite Difference [16],[17], Virtual Element Methods (VEM) [18], Finite Volumes [19] and Discontinuous Galerkin Methods [20]. The mimetic finite difference is casted within the variational framework, whereas, the VEM approach is consistent and stable finite element method[21], [22]. Hence, the VEM exactly passes the patch

S. Natarajan[a]

[a]Department of Mechanical Engineering, Indian Institute of Technology, Madras, Chennai - 600036.
E-mail: snatarajan@cardiffalumni.org.uk; snatarajan@iitm.ac.in.

S. P. A. Bordas[c,d,e]

[c] Faculté des Sciences, de la Technologie et de la Communication, University of Luxembourg, Luxembourg.
[d]Theoretical and Applied Mechanics, School of Engineering, Cardiff University, Cardiff CF24 3AA, Wales, UK.
[e]Department of Mechanical Engineering, University of Western Australia, Australia.

test over polygonal and polyhedral finite elements and does not require any explicit construction of the basis functions. Interested readers are redirected to [23],[24],[25],[26]. The arbitrary polytopes uses rational basis functions which are non-polynomial basis functions. Some of the interpolants over arbitrary polytopes are: Mean value coordinates [27], Harmonic shape functions [28], Laplace basis functions [29] and maximum entropy basis functions [30]. Recently, Ooi et. al. [31] worked on the construction of interpolants over arbitrary polytopes using the Scaled Boundary Finite Element method (SBFEM). Inspite of all these merits, the PFEM faces the issue of numerical integration and does not pass the patch test [32],[33] upto the machine precision. This is due to the sub-optimal procedure adopted for the numerical integration over arbitrary polytopes, wherein each polytope is divided into triangles (in two dimensions) or tetrahedron (in three dimensions) and the usual quadrature scheme are employed over them. It is also seen that the strain smoothing technique proposed by Chen et al. [34] for the meshfree methods is one of the efficient technique of numerical integration. The key feature of the strain smoothing is the conversion of the volume integration into the surface integration using the Gauss divergence theorem and evaluate the stiffness matrix with the information of the nodal shape functions only. This gives flexibility in finite element mesh topology due to the absence of Jacobian. The smoothed strain are evaluated at the centroid of each subcell which can only reproduce a constant strain field in the cell. This technique was further extented to the conventional FEM by Liu et al. [35] and named this method as Smoothed Finite Element Method (SFEM). The SFEM are categorized according to the construction of the smoothing cell; for example, the Cell-based Smoothed FEM (CS-FEM) [35],[36], the Node-based Smoothed FEM (NS-FEM) [37] and the Edge-based Smoothed FEM (ES-FEM) [38],[39], Face-based Smoothed FEM (FS-FEM) [35] and α-FEM [40]. With SFEM Liu et al. [35] concluded that the performance of the finite elements is improved in comparision to the conventional FEM. Later, when the SFEM was applied over arbitrary polytopes and higher order finite elements, it yields sub-optimal convergence compared to the conventional method present to solve these elements [41],[42]. With respect to the above issue and inspired by the recent work of Duan et al. [43],[44],[45], Chen et al. [34] and Liu et al. [35] a modified strain smoothing technique named LS scheme is presented in our previous paper [1]. The LS scheme leads to improve the accuracy and recovers optimal convergence for the arbitrary convex polytopes and higher order elements. The smoothing function chosen is linear polynomial basis over each subcell. Similar to CSFEM, the modified strain computed over these smoothing cells is used to compute the stiffness matrix. The number of terms used in the smoothing function decides the number of Gauss points required for the numerical integration. Thus, minimum three Gauss points are used within the triangular subcell, whereas four gauss points are used with the quadrilateral subcells in two dimensions. The modified derivative used to computed the stiffness matrix are evaluated at each of the Gauss point. Recently, Natarajan et. al. [26] had showed the connection between the SFEM and VEM over arbitrary polytopes.

In this paper, we present a new one point quadrature rule over arbitrary star convex polytopes which reproduce linear strain using only one centroidal point of each subcell during numerical integration improving the accuracy and convergence properties of arbitrary polytopes. In order to do achieve this characteristic, the Taylor's expansion of the stiffness matrix is employed. The modified higher order derivatives of the shape function is used. These modified derivatives are obtained at the centroid of each subcell and assembled to compute the stiffness matrix. The use of these modified derivatives at the quadrature points provide stability according to the consistency frame work for the nodal derivatives shown in [43]. The key feature of this paper is to produce the linear strain using the Taylor's expansion of the stiffness matrix and using modified higher order derivatives of shape function at the centroid of each subcell rather than using the three quadrature point to evaluate the modified derivatives used to compute the stiffness matrix.

2 Strong and weak form for a linear elastic media

Consider an isotropic linear elastic body situated in $d = 2, 3$ dimensional space defined by an open domain $\Omega \subset \mathbb{R}^d$, bounded by the $(d{-}1)$ dimensional surface Γ such that $\Gamma = \Gamma_u \cup \Gamma_t$ and $\emptyset = \Gamma_u \cap \Gamma_t$, where Γ_u is the Dirichlet boundary and Γ_t is the Neumann boundary whose unit outward normal is $\mathbf{n}$. The boundary-value problem for linear elastostatics is defined by

$$\boldsymbol{\nabla} \cdot \boldsymbol{\sigma} + \mathbf{b} = \mathbf{0} \ \forall \mathbf{x} \in \Omega, \tag{1a}$$

$$\mathbf{u} = \hat{\mathbf{u}} \ \forall \mathbf{x} \in \Gamma_u, \tag{1b}$$

$$\boldsymbol{\sigma} \cdot \mathbf{n} = \hat{\mathbf{t}} \ \forall \mathbf{x} \in \Gamma_t, \tag{1c}$$

where $\boldsymbol{\sigma}$ is the Cauchy stress tensor and $\mathbf{u} : \Omega \to \mathbb{R}^d$ be the displacement field at a point $\mathbf{x}$ of the elastic body when the body is subjected to external tractions $\bar{\mathbf{t}} : \Gamma_t \to \mathbb{R}^d$ and body forces $\mathbf{b} : \Omega \to \mathbb{R}^d$. The

corresponding weak form is:

$$a(\mathbf{u}, \mathbf{v}) = \ell(\mathbf{v}) \ \forall \mathbf{v} \in \mathscr{V}, \tag{2a}$$

$$a(\mathbf{u}, \mathbf{v}) = \int_{\Omega} \boldsymbol{\sigma}(\mathbf{u}) : \boldsymbol{\varepsilon}(\mathbf{v}) \, dV, \tag{2b}$$

$$\ell(\mathbf{v}) = \int_{\Omega} \mathbf{b} \cdot \mathbf{v} \, dV + \int_{\Gamma_t} \hat{\mathbf{t}} \cdot \mathbf{v} \, dS, \tag{2c}$$

where $\boldsymbol{\varepsilon}$ is the small strain tensor. To find $\mathbf{u} \in \mathscr{U}$ such that $\mathscr{U}$ and $\mathscr{V}$ are the displacement trial and test spaces respectively:

$$\mathscr{U} := \left\{ \mathbf{u}(\mathbf{x}) \in [C^0(\Omega)]^d : \mathbf{u} \in [\mathcal{W}(\Omega)]^d \subseteq [H^1(\Omega)]^d, \ \mathbf{u} = \hat{\mathbf{u}} \text{ on } \Gamma_u \right\},$$

$$\mathscr{V} := \left\{ \mathbf{v}(\mathbf{x}) \in [C^0(\Omega)]^d : \mathbf{v} \in [\mathcal{W}(\Omega)]^d \subseteq [H^1(\Omega)]^d, \ \mathbf{v} = \mathbf{0} \text{ on } \Gamma_u \right\},$$

where the space $\mathcal{W}(\Omega)$ includes linear displacement fields. The domain is partitioned into elements Ω^h, and on using shape functions ϕ that span at least the linear space. The vector-valued trial and test functions $\mathbf{u}^h = \sum_{e=1}^{nn_{el}} \phi_e \mathbf{u}_e$ and $\mathbf{v}^h = \sum_{e=1}^{nn_{el}} \phi_e \mathbf{v}_e$, respectively, issubstitute into Equation (2) and apply a standard Galerkin procedure to obtain the discrete weak form to find $\mathbf{u}^h \in \mathscr{U}^h$ such that

$$a(\mathbf{u}^h, \mathbf{v}^h) = \ell(\mathbf{v}^h) \ \forall \mathbf{v}^h \in \mathscr{V}^h, \tag{4}$$

which leads to the following system of linear equations:

$$\mathbf{K} \mathbf{u} = \mathbf{f}, \tag{5a}$$

$$\mathbf{K} = \sum_h \mathbf{K}^h = \sum_h \int_{\Omega^h} \mathbf{B}^{\mathrm{T}} \mathbf{C} \mathbf{B} \, dV, \tag{5b}$$

$$\mathbf{f} = \sum_h \mathbf{f}^h = \sum_h \left(\int_{\Omega^h} \boldsymbol{\phi}^{\mathrm{T}} \mathbf{b} \, dV + \int_{\Gamma_t^h} \boldsymbol{\phi}^{\mathrm{T}} \hat{\mathbf{t}} \, dS \right), \tag{5c}$$

where $\mathbf{K}$ is the global assembled stiffness matrix, $\mathbf{f}$ is the global assembled nodal force vector, $\mathbf{u}$ the global assembled vector of nodal displacements, ϕ is the matrix of shape functions, $\mathbf{C}$ is the constitutive matrix for an isotropic linear elastic material, and $\mathbf{B} = \boldsymbol{\nabla}_s \phi$ is the strain-displacement matrix that is computed using the derivatives of the shape functions.

The shape functions over arbitrary polytopes are collectively called as 'barycentric coordinates'. There are different ways to represent the shape function over arbitrary polytopes [2]. In this paper, Wachspress interpolants are used over arbitrary polytopes. The polygonal/polyhedral finite elements demands the construction of sufficiently accurate integration rules for computing the stiffness matrix defined in Equation (5). In this effort, a modified strain-displacement matrix is defined to compute the stiffness matrix. This modified strain-displacement matrix is denoted by $\tilde{\mathbf{B}}$ and is constructed using the smoothing cells. A smoothing technique that yields linear strain and improves the accuracy in the polygonal/polyhedral finite elements using $3n$ integration point is compared with the smoothing technique that yields linear strain and improves accuracy in polygonal/polyhedral finite elements using n integration point is proposed in this paper. Where n denotes the number of integration cell within a polytope. The comparision is also made with the constant smoothing technique that yields constant strain within subcell. The stable and efficient numerical integration using n integration point of the Galerkin weak form is obtained by performing the Taylor's expansion of the modified stiffness matrix within the smoothing cells as shown in Equation (7b), which is explained in the next section briefly with notations.

$$\tilde{\mathbf{K}} = \sum_h \tilde{\mathbf{K}}^h = \sum_h \int_{\Omega^h} \tilde{\mathbf{B}}^{\mathrm{T}} \mathbf{C} \tilde{\mathbf{B}} \, dV, \tag{6}$$

$$\tilde{\mathbf{K}}^{\Omega_c} = \int_{\Omega_c} \tilde{\mathbf{B}}^{\mathrm{T}} \mathbf{C} \tilde{\mathbf{B}} \, dV, \tag{7a}$$

$$= \int_{\Omega_c} \left[\tilde{\mathbf{B}}^{\mathrm{T}} + \frac{\partial \tilde{\mathbf{B}}^{\mathrm{T}}}{\partial x}(x - x_c) + \frac{\partial \tilde{\mathbf{B}}^{\mathrm{T}}}{\partial y}(y - y_c) \right] \times \mathbf{C}$$

$$\times \left[\tilde{\mathbf{B}}^{\mathrm{T}} + \frac{\partial \tilde{\mathbf{B}}^{\mathrm{T}}}{\partial x}(x - x_c) + \frac{\partial \tilde{\mathbf{B}}^{\mathrm{T}}}{\partial y}(y - y_c) \right] dV, \tag{7b}$$

The constant smoothing technique and linear smoothing technique using $3n$ integration points can be expressed using Equation (7a), where only the matrix $\tilde{\mathbf{B}}$ varies, with a linear smoothed strain-displacement operator shown in [1] as opposed to a constant smoothed strain-displacement operator shown in [35, 26]. While the Taylor's expansion of the Equation (7a), expressed by the Equation (7b) is used for the linear smoothing technique with $1n$ integration points where n is the number of smoothing cells within an arbitrary polytopes.

3 One point quadrature scheme

The main focus of this paper is to further extend the linear smoothing technique using just one point of integration per smoothing cell rather than three integration points as used in our earlier study [1]. The basic idea is to compute the modified strain-displacement matrix used to construct the modified stiffness matrix Equation (6). To this end, we rely on the smoothed finite element method, which has its origin in the stabilized conforming nodal integration [34] for meshfree methods, where the strain field is sampled at the nodes by smoothing the nodal strain on the boundary of a representative nodal volume ('the smoothed domain'). In particular, we focus our attention on the cell-based smoothing technique. In the CSFEM, the elements are divided into subcells as shown in Figure 2. Triangles in two dimensions and tetrahedra in three dimensions is used. The strain smoothing technique is then applied within each subcell to evaluate the modified strain. For simplicity of the notation, the derivation of the smoothing scheme is given in detail only for two-dimensions using the Cartesian coordinate system. In addition, n_j $(j = 1, 2)$ is the j-th component of the unit outward normal to a cell edge in the Cartesian coordinate system. The discrete modified strain field $\tilde{\varepsilon}_{ij}^h$ that yields the modified strain-displacement matrix ($\tilde{\mathbf{B}}$) that is used to build the stiffness matrix is computed by satisfying the orthogonality condition between the compatible and the smoothed nodal derivatives at the point of integration, given as;

$$\int_{\Omega_C^h} q(\mathbf{x}) \left(\phi_{I,x} - \tilde{\phi}_{I,x} \right) \ \mathrm{d}V = 0 \tag{8}$$

where $q(\mathbf{x})$ is a smoothing function. The above Equation (8) can be rewritten as;

$$\int_{\Omega_C^h} \tilde{\phi}_{I,x} \ q(\mathbf{x}) \ \mathrm{d}\Omega = \int_{\Omega_C^h} \phi_{I,x} \ q(\mathbf{x}) \ \mathrm{d}V \tag{9}$$

On writing Equation (9) at the basis functions derivatives level, its right-hand side can be expressed in terms of the divergence theorem, as follows:

$$\int_{\Omega_C^h} \phi_{I,x} \ q(\mathbf{x}) \, \mathrm{d}V = \int_{\Gamma_C^h} \phi_I \ q(\mathbf{x}) n_j \, \mathrm{d}S - \int_{\Omega_C^h} \phi_I \ q_{,x}(\mathbf{x}) \, \mathrm{d}V \tag{10}$$

Equation (10) was coined as *divergence consistency* in Duan et al. [43, 44, 45], where it was introduced to correct integration errors in second- and third-order meshfree approximations. This divergence consistency was later used by Sukumar to correct integration errors in quadratic maximum-entropy serendipity polygonal elements [46] and by Ortiz-Bernardin and co-workers to correct integration errors in the volume-averaged nodal projection (VANP) meshfree method [47, 48].

The interpolated standard strain field $\boldsymbol{\varepsilon}^h$ and modified strain field $\tilde{\boldsymbol{\varepsilon}}^h$ is approximated by the displacement field as follows:

$$\boldsymbol{\varepsilon}^h = \mathbf{B}\mathbf{u}$$

$$\tilde{\boldsymbol{\varepsilon}}^h = \tilde{\mathbf{B}}\mathbf{u}$$

Thus, the modified strain field $\tilde{\varepsilon}_{ij}^h$ and the standard compatible strain field ε_{ij}^h in each Ω_C^h, is related as follows:

$$\tilde{\varepsilon}_{ij}^h(\mathbf{x}) = \int_{\Omega_C^h} \varepsilon_{ij}^h(\mathbf{x}) \ q(\mathbf{x}) \mathrm{d}V \tag{11}$$

Equation (10) is used to evaluated the modified derivatives. In the CSFEM [35] $q(\mathbf{x}) = [1]$ is used, this is only consistent for linear approximation. The modified strain $\tilde{\phi}_{I,x}(x_c)$ is used to evaluate the modified stiffness matrix for constant smoothing technique. Futhermore, if $q(\mathbf{x}) = [1 \ x \ y]$ which is the key feature in the formulation of linear smoothing technique presented in our previous study [1], which allows to be consistent in higher order approximation. In the linear smoothing technique, the modified strain using $3n$ integration
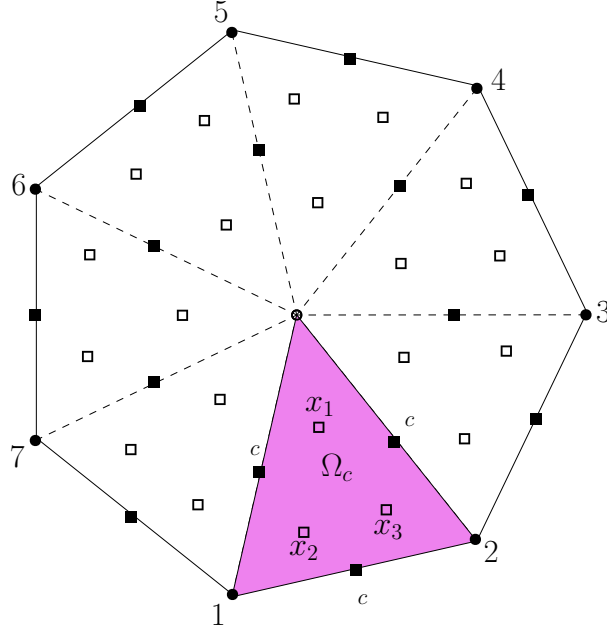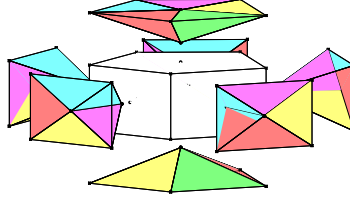
(a) Number of integration point used per subcell with three point integration rule
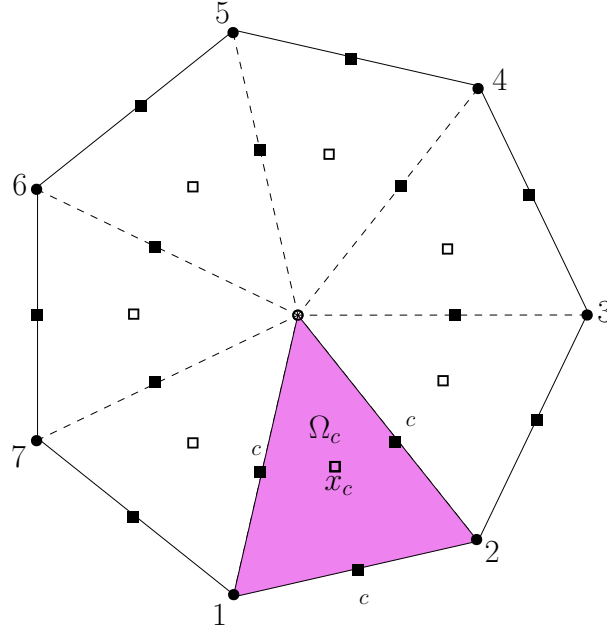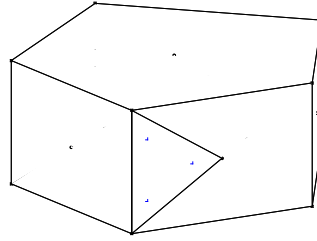

(b) Number of integration point used per subcell with one point integration rule

Fig. 1: Schematic representation of the three point and one point integration techniques. The nodes are depicted by the filled circles, while the Gauss point per edge is shown by filled squares. The smoothed derivatives are computed at the 'open' squares over each smoothing cell denoted by Ω_c. Discertization of arbitrary polygon into triangular subcell using virtual point shown by 'open' circle.

points i.e. $\tilde{\phi}_{I,x}(x_1), \tilde{\phi}_{I,x}(x_2), \tilde{\phi}_{I,x}(x_3)$ where n is the number of edges of the arbitrary polygon and x_1, x_2 and x_3 are the integration points within each smoothing cells shown by open square in Figure 2 (b). So, in order to minimize the quadrature for numerical integration we are presenting one point integration scheme for the same $q(\mathbf{x})$ over the same smoothing domain. This is done by using Taylor's expansion of the weak form and using the smoothed higher order derivatives in the weak form i.e $\tilde{\phi}_{I,x}(x_c), \tilde{\phi}_{I,xx}(x_c), \tilde{\phi}_{I,xy}(x_c)$.

(a)Discretization of arbitrary polyhedron with tetrahedron subcell using virtual node shown by open circle.

(b) Number of integration point used per subcell with four point integration rule
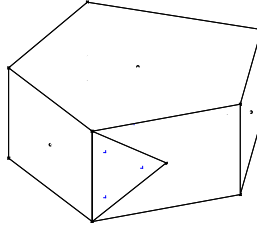
(c) Number of integration point used per subcell with one point integration rule

Fig. 2: Schematic representation of the four point and one point integration techniques. The nodes are depicted by the black open square, while the Gauss point per surface is shown by blue open squares. The smoothed derivatives are computed at the 'star' over each smoothing cell denoted by Ω_c.

To introduce the high order derivatives into Equation (6), the Taylor's expansion of $\tilde{\phi}_{I,x}(\mathbf{x})$, $\mathbf{q}(\mathbf{x})$ and $\phi_I(\mathbf{x})$, used is defined as:

$$\tilde{\phi}_{I,x}(\mathbf{x}) = \tilde{\phi}_{I,x}(\mathbf{x}_c) + (x - x_c)\tilde{\phi}_{I,xx}(\mathbf{x}_c) + (y - y_c)\tilde{\phi}_{I,xy}(\mathbf{x}_c) + \mathcal{O}((\mathbf{x} - \mathbf{x}_c)^2) \tag{12}$$

$$\mathbf{q}(\mathbf{x}) = \mathbf{q}(\mathbf{x}_c) + (x - x_c)\mathbf{q}_{,x}(\mathbf{x}) + (y - y_c)\mathbf{q}_{,y}(\mathbf{x}) \tag{13}$$

$$\phi_I(\mathbf{x}) = \phi_I(\mathbf{x}_c) + (x - x_c)\phi_{I,x}(\mathbf{x}_c) + (y - y_c)\phi_{I,y}(\mathbf{x}_c) + \frac{1}{2}(x - x_c)^2\phi_{I,xx}(\mathbf{x}_c)$$
$$+ (x - x_c)(y - y_c)\phi_{I,xy}(\mathbf{x}_c) + \frac{1}{2}(y - y_c)^2\phi_{I,yy}(\mathbf{x}_c) + \mathcal{O}((\mathbf{x} - \mathbf{x}_c)^3) \tag{14}$$

where $\mathbf{x}_c = \{x_c, y_c\}$ Figure 2 is the center of the cell. Upon substituting Equation (14) into Equation (10), we have:

$$\mathbf{q}(\mathbf{x}_c)A\tilde{\phi}_{I,x}(\mathbf{x}_c) + \left[\mathbf{q}_x(\mathbf{x}_c)I_c^{xx} + \mathbf{q}_y(\mathbf{x}_c)I_c^{xy}\right]\tilde{\phi}_{I,xx}(\mathbf{x}_c) + \left[\mathbf{q}_{,x}(\mathbf{x}_c)I_c^{xy} + \mathbf{q}_{,y}(\mathbf{x}_c)I_c^{yy}\right]\tilde{\phi}_{I,xy}(\mathbf{x}_c)$$
$$= \int_{\Gamma_c} \phi_I(\mathbf{x})\mathbf{q}(\mathbf{x})\mathbf{n}\,\mathrm{d}\Gamma - \left[A\phi_I(\mathbf{x}_c) + \frac{1}{2}I_c^{xx}\phi_{I,xx}(\mathbf{x}_c) + I_c^{xy}\phi_{I,xy}(\mathbf{x}_c) + \frac{1}{2}I_c^{yy}\phi_{I,yy}(\mathbf{x}_c)\right] \tag{15}$$

where $A = \int\limits_{\Omega_c} \mathrm{d}\Omega$ is the area of the integration domain Ω. The first order area moments with respect to cell center $\mathbf{x}_c$ vanish and the second order area moments are given by:

$$
\begin{Bmatrix} I_c^{xx} \\ I_c^{xy} \\ I_c^{yy} \end{Bmatrix} = \int\limits_{\Omega_c} \begin{Bmatrix} (x - x_c)^2 \\ (x - x_c)(y - y_c) \\ (y - y_c)^2 \end{Bmatrix} \mathrm{d}\Omega \tag{16}
$$

Remark 1 For a regular polygon, the second order area moment I_c^{xy} also vanish apart from the first order area moments.

For $\mathbf{q}(\mathbf{x}) = \begin{bmatrix} 1 & x & y \end{bmatrix}$ and using numerical integration to evaluate the boundary integral, Equation (15) leads to the following system of linear equations:

$$
\mathbf{W}\mathbf{d}_j = \mathbf{f}_j, \quad j = 1, 2 \tag{17}
$$

where,

$$
\mathbf{W} = \begin{bmatrix} A & 0 & 0 \\ Ax_c & I_c^{xx} & I_c^{xy} \\ Ay_c & I_c^{xy} & I_c^{yy} \end{bmatrix} \tag{18a}
$$

$$
\mathbf{f}_1 = \begin{Bmatrix} \sum\limits_{L=1}^{3} \sum\limits_{G=1}^{2} \phi_I(\mathbf{x}_G) n_x^L w_G \\ \sum\limits_{G=1}^{2} \phi_I(\mathbf{x}_G) x_G n_x^L w_G - Fg \\ \sum\limits_{G=1}^{2} \phi_I(\mathbf{x}_G) y_G n_x^L w_G \end{Bmatrix} \tag{18b}
$$

$$
\mathbf{f}_2 = \begin{Bmatrix} \sum\limits_{L=1}^{3} \sum\limits_{G=1}^{2} \phi_I(\mathbf{x}_G) n_x^L w_G \\ \sum\limits_{G=1}^{2} \phi_I(\mathbf{x}_G) x_G n_x^L w_G \\ \sum\limits_{G=1}^{2} \phi_I(\mathbf{x}_G) y_G n_x^L w_G - Fg \end{Bmatrix} \tag{18c}
$$

where $Fg = A\phi_I(\mathbf{x}_c) + \frac{1}{2} I_c^{xx} \phi_{I,xx}(\mathbf{x}_c) + I_c^{xy} \phi_{I,xy}(\mathbf{x}_c) + \frac{1}{2} I_c^{yy} \phi_{I,yy}(\mathbf{x}_c)$ and $\phi_I(\mathbf{x}_c)$, $\phi_{I,xx}(\mathbf{x}_c)\,\phi_{I,yy}(\mathbf{x}_c)$ and $\phi_{I,xy}(\mathbf{x}_c)$ are the barycentric coordinates and its derivatives are evaluated at the center of the cell. The x_G, y_G and w_G are the integration points and weights respectively, along the boundary of the smoothing cells shown by filled square in Figure 2 and n_x^L are the outward normals along the smoothing cell boundaries.

The solution vector is given by:

$$
\mathbf{d}_1 = \begin{Bmatrix} \tilde{\phi}_{I,x}(\mathbf{x}_c) \\ \tilde{\phi}_{I,xx}(\mathbf{x}_c) \\ \tilde{\phi}_{I,xy}(\mathbf{x}_c) \end{Bmatrix} \tag{19a}
$$

$$
\mathbf{d}_2 = \begin{Bmatrix} \tilde{\phi}_{I,y}(\mathbf{x}_c) \\ \tilde{\phi}_{I,yx}(\mathbf{x}_c) \\ \tilde{\phi}_{I,yy}(\mathbf{x}_c) \end{Bmatrix} \tag{19b}
$$

This is further used to construct the modified strain displacement matrix and its derivatives used to evaluate the stiffness matrix as:

$$
\tilde{\mathbf{B}} = \begin{bmatrix} \tilde{\mathbf{B}}_1 & \tilde{\mathbf{B}}_2 & .... & \tilde{\mathbf{B}}_n \end{bmatrix} \tag{20}
$$

$$
\tilde{\mathbf{B}}_I(\mathbf{x}_c) = \begin{bmatrix} \tilde{\phi}_{I,x}(\mathbf{x}_c) & 0 \\ 0 & \tilde{\phi}_{I,y}(\mathbf{x}_c) \\ \tilde{\phi}_{I,y}(\mathbf{x}_c) & \tilde{\phi}_{I,x}(\mathbf{x}_c) \end{bmatrix} \tag{21}
$$

$$
\frac{\partial \tilde{\mathbf{B}}_I(\mathbf{x}_c)}{\partial x} = \begin{bmatrix} \tilde{\phi}_{I,xx}(\mathbf{x}_c) & 0 \\ 0 & \tilde{\phi}_{I,yx}(\mathbf{x}_c) \\ \tilde{\phi}_{I,yx}(\mathbf{x}_c) & \tilde{\phi}_{I,xx}(\mathbf{x}_c) \end{bmatrix} \tag{22}
$$

$$\frac{\partial \tilde{\mathbf{B}}_I(\mathbf{x}_c)}{\partial y} = \begin{bmatrix} \tilde{\phi}_{I,xy}(\mathbf{x}_c) & 0 \\ 0 & \tilde{\phi}_{I,yy}(\mathbf{x}_c) \\ \tilde{\phi}_{I,yy}(\mathbf{x}_c) & \tilde{\phi}_{I,xy}(\mathbf{x}_c) \end{bmatrix} \tag{23}$$

It should be noted that in the proposed technique the smoothed nodal derivative is only used in evaluation of the modified stiffness matrix Equation (6) and the standard Waschpress shape function derivatives are used for computing the body force as given by Equation (24).

$$\mathbf{f^b} = \int_{\Omega_c} \left(\boldsymbol{\phi}^{\mathrm{T}} \mathbf{b} \right) \mathrm{d}V, \tag{24a}$$

$$= \int_{\Omega_c} \left\{ \boldsymbol{\phi}^{\mathrm{T}} \mathbf{b}|_{(\mathbf{x}_c)} + \frac{\partial \boldsymbol{\phi}^{\mathrm{T}}}{\partial x} \mathbf{b}|_{(\mathbf{x}_c)}(x - x_c) + \frac{\partial \boldsymbol{\phi}^{\mathrm{T}}}{\partial y} \mathbf{b}|_{(\mathbf{x}_c)}(y - y_c) \right.$$

$$+ \frac{1}{2} \frac{\partial^2 \boldsymbol{\phi}^{\mathrm{T}}}{\partial x^2} \mathbf{b}|_{(\mathbf{x}_c)}(x - x_c)^2 + \frac{1}{2} \frac{\partial^2 \boldsymbol{\phi}^{\mathrm{T}}}{\partial y^2} \mathbf{b}|_{(\mathbf{x}_c)}(y - y_c)^2 \tag{24b}$$

$$\left. + \frac{\partial^2 \boldsymbol{\phi}^{\mathrm{T}}}{\partial x \partial y} \mathbf{b}|_{(\mathbf{x}_c)}(y - y_c)(y - y_c) \right\} \, \mathrm{d}V,$$

$$= \mathbf{A} \boldsymbol{\phi}^{\mathrm{T}} \mathbf{b}|_{(\mathbf{x}_c)} + \frac{1}{2} I_c^{xx} \frac{\partial^2 \boldsymbol{\phi}^{\mathrm{T}}}{\partial x^2} \mathbf{b}|_{(\mathbf{x}_c)} + \frac{1}{2} I_c^{yy} \frac{\partial^2 \boldsymbol{\phi}^{\mathrm{T}}}{\partial y^2} \mathbf{b}|_{(\mathbf{x}_c)} + I_c^{xy} \frac{\partial^2 \boldsymbol{\phi}^{\mathrm{T}}}{\partial x \partial y} \mathbf{b}|_{(\mathbf{x}_c)} \tag{24c}$$

Remark 2 Equation (17) always have an unique solution provided the triangles do not degenerate to a line.

4 Numerical examples

In this section, we study the accuracy and the convergence properties of the proposed linear smoothing scheme (LS) over arbitrary polytopes using $1n$ integration point. The LS scheme is compared to the constant smoothing (CS) scheme by solving few benchmark problems. We also demonstrate the performance of the proposed scheme in a simple three-dimensional elasticity problem. In all the numerical examples, we discretize the domain with arbitrary polytope based on centroid Voronoi tessellation. The following convention is used while discussing the results:

– CS: constant smoothing over arbitrary polygons in two dimensions.
– LS3n-2D, LS3n-3D: linear smoothing scheme with three point integration rule over arbitrary polytopes, in two and in three dimensions, respectively.
– LS1-2D, LS1-3D: linear smoothing scheme with one point integration rule over arbitrary polytopes, in two and three dimensions, respectively.

For the above integration scheme, the elements are sub-divided into triangles or tetrahedra in two and three dimensions, called as smoothing cells. The linear smoothing scheme is then performed over each smoothing cells. For the purpose of error estimation and convergence studies, the L^2 norm and H^1 seminorm of the error are used.

4.1 Patch test

In the first example, the accuracy and the convergence properties of the proposed one point quadrature (LS1-2D, LS1-3D) is demonstrated with a linear and a quadratic patch test.

Linear patch test The following displacements are prescribed on the boundary in the two-dimensional case:

$$\begin{pmatrix} \hat{u} \\ \hat{v} \end{pmatrix} = \begin{pmatrix} 0.1 + 0.1x + 0.2y \\ 0.05 + 0.15x + 0.1y \end{pmatrix} \tag{25}$$

and in the three-dimensional case the following displacements are prescribed on the boundary:

$$\begin{pmatrix} \hat{u} \\ \hat{v} \\ \hat{w} \end{pmatrix} = \begin{pmatrix} 0.1 + 0.1x + 0.2y + 0.2z \\ 0.05 + 0.15x + 0.1y + 0.2z \\ 0.05 + 0.1x + 0.2y + 0.2z \end{pmatrix}. \tag{26}$$

The exact solution to Equation (1) is $\mathbf{u} = \hat{\mathbf{u}}$ in the absence of body forces. The domain is discretized with arbitrary polygonal and polyhedral finite elements. Figure 3 and Figure 4 shows a few representative
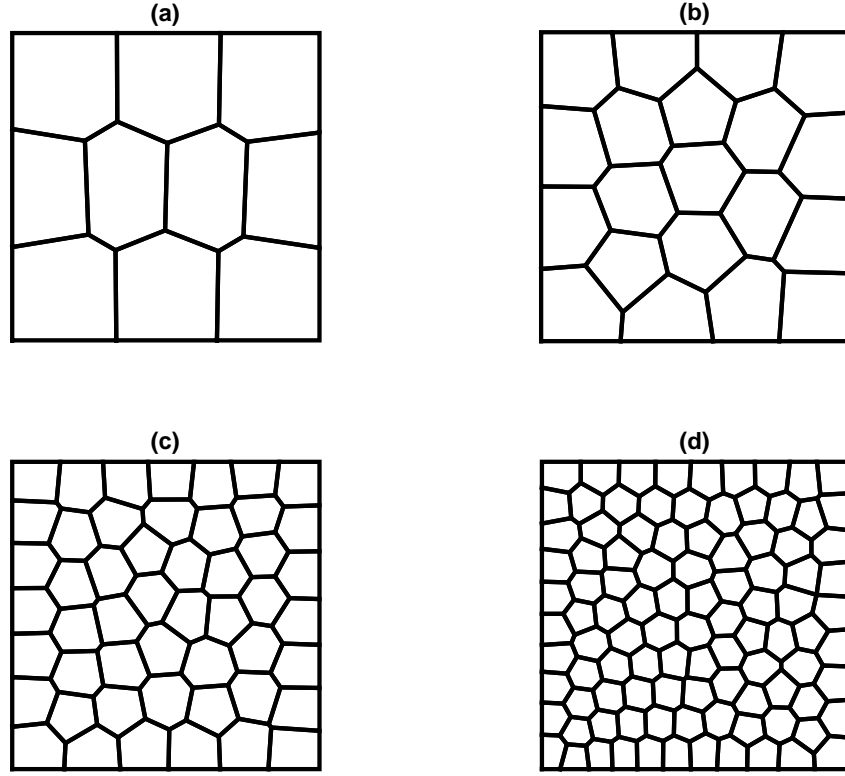
Fig. 3: Square domain discretized with polygonal elements. Representative meshes containing (a) 10, (b) 20, (c) 50 and (d) 100 polygons.

Table 1: Error in the L^2 norm and H^1 seminorm for the two-dimensional linear patch test.

Mesh	CS		LS3n-2D		LS1-2D	
	L^2	H^1	L^2	H^1	L^2	H^1
a	1.7334×10^{-07}	2.3328×10^{-05}	5.3835×10^{-14}	2.8388×10^{-11}	8.3750×10^{-15}	2.9603×10^{-13}
b	1.6994×10^{-07}	3.4094×10^{-05}	1.9255×10^{-13}	4.4373×10^{-11}	7.6187×10^{-14}	4.7876×10^{-12}
c	7.2017×10^{-07}	2.2573×10^{-04}	2.0030×10^{-13}	7.0017×10^{-11}	1.4322×10^{-13}	1.2796×10^{-11}
d	7.4144×10^{-07}	2.5773×10^{-04}	2.9567×10^{-13}	1.0199×10^{-10}	2.7035×10^{-13}	2.7567×10^{-11}

Table 2: Error in the L^2 norm and H^1 seminorm for the three-dimensional linear patch test.

Mesh (c.f. Figure 4)	LS3n-3D		LS1-3D	
	L^2	H^1	L^2	H^1
a	2.0280×10^{-12}	3.3428×10^{-10}	2.9862×10^{-11}	2.2225×10^{-10}
b	1.9218×10^{-12}	1.7529×10^{-10}	7.3836×10^{-10}	5.5601×10^{-09}
c	2.6660×10^{-12}	4.9320×10^{-10}	2.0818×10^{-10}	2.1329×10^{-09}
d	3.2074×10^{-12}	3.1083×10^{-10}	7.7299×10^{-10}	1.2843×10^{-09}

meshes used for the two and three dimensional studies, respectively. The errors in the L^2 norm and the H^1 seminorm for the CS, LS3n schemes and the proposed LS1 one point quadrature are shown in Table 1 for two-dimensions and in Table 2 for three dimensions. It can be seen that the proposed one point quadrature scheme passes the linear patch test to machine precision for both polygonal and polyhedral discretizations.
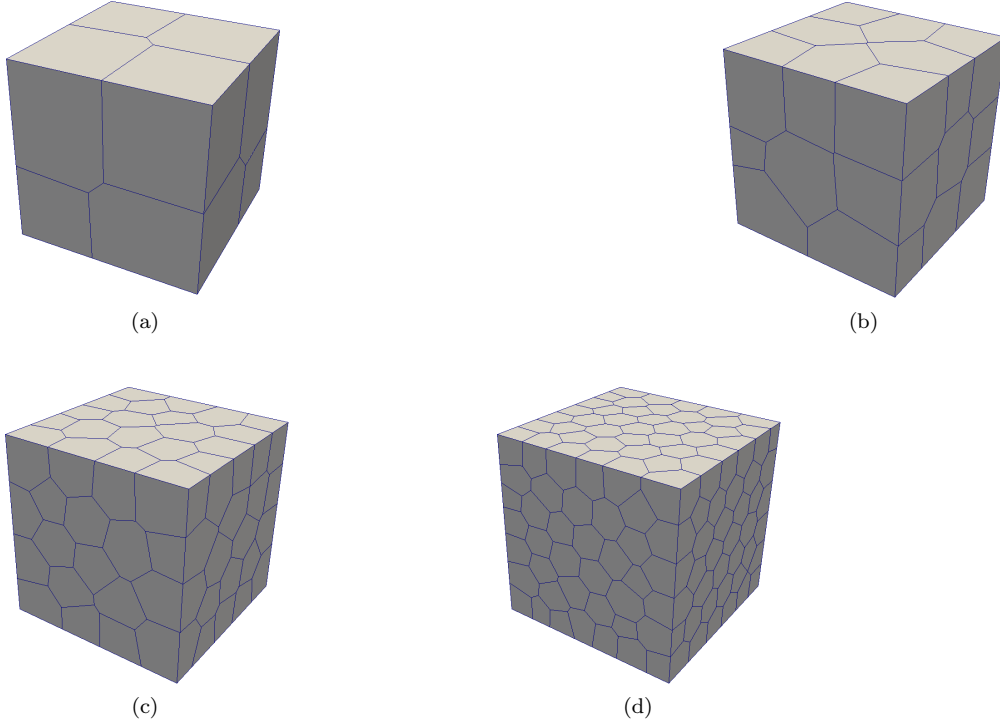
Fig. 4: Cube domain discretized with polyhedral elements. Representative meshes containing (a) 7, (b) 25, (c) 100 and (d) 300 polyhedra.

Quadratic patch test In the quadratic patch test, the following displacements are prescribed on the boundaries for the two-dimensional case:

$$\begin{pmatrix} \hat{u} \\ \hat{v} \end{pmatrix} = \begin{pmatrix} 0.1x^2 + 0.1xy + 0.2y^2 \\ 0.05x^2 + 0.15xy + 0.1y^2 \end{pmatrix}, \tag{27}$$

and the following in the three-dimensional case:

$$\begin{pmatrix} \hat{u} \\ \hat{v} \\ \hat{w} \end{pmatrix} = \begin{pmatrix} 0.1 + 0.2x + 0.2x + 0.1z + 0.15x^2 + 0.2y^2 + 0.1z^2 + 0.15xy + 0.1yz + 0.1zx \\ 0.15 + 0.1x + 0.1y + 0.2z + 0.2x^2 + 0.15y^2 + 0.1z^2 + 0.2xy + 0.1yz + 0.2zx \\ 0.15 + 0.15x + 0.2y + 0.1z + 0.15x^2 + 0.1y^2 + 0.2z^2 + 0.1xy + 0.2yz + 0.15zx \end{pmatrix} \tag{28}$$

The exact solution to Equation (1) is $\mathbf{u} = \hat{\mathbf{u}}$ when the body is subjected to the body forces:

$$\mathbf{b} = \begin{pmatrix} -0.2\mathbf{C}(1,1) - 0.15\mathbf{C}(1,2) - 0.55\mathbf{C}(3,3) \\ -0.1\mathbf{C}(1,2) - 0.2\mathbf{C}(2,2) - 0.2\mathbf{C}(3,3) \end{pmatrix}, \tag{29}$$

in two-dimensions and

$$\mathbf{b} = \begin{pmatrix} -0.3\mathbf{C}(1,1) - 0.2\mathbf{C}(1,2) - 0.15\mathbf{C}(1,3) - 0.6\mathbf{C}(4,4) - 0.35\mathbf{C}(6,6) \\ -0.15\mathbf{C}(1,2) - 0.3\mathbf{C}(2,2) - 0.2\mathbf{C}(2,3) - 0.55\mathbf{C}(4,4) - 0.4\mathbf{C}(5,5) \\ 0.1\mathbf{C}(1,3) - 0.1\mathbf{C}(2,3) - 0.4\mathbf{C}(3,3) - 0.3\mathbf{C}(5,5) - 0.4\mathbf{C}(6,6) \end{pmatrix} \tag{30}$$

in three dimensions, where $\mathbf{C}$ is the constitutive matrix. Figure 5 shows the convergence rates when the domain is discretized with polyhedral linear elements. It can be inferred that the proposed one point quadrature scheme yields optimal convergence rates.

4.2 Thick cantilever beam under end shear

In this example, a two-dimensional cantilever beam subjected to a parabolic shear load at the free end is examined, as shown in Figure 6. The geometry of the cantilever is $L = 10$ m and $D = 2$ m. The material

(a) Two dimensional domain

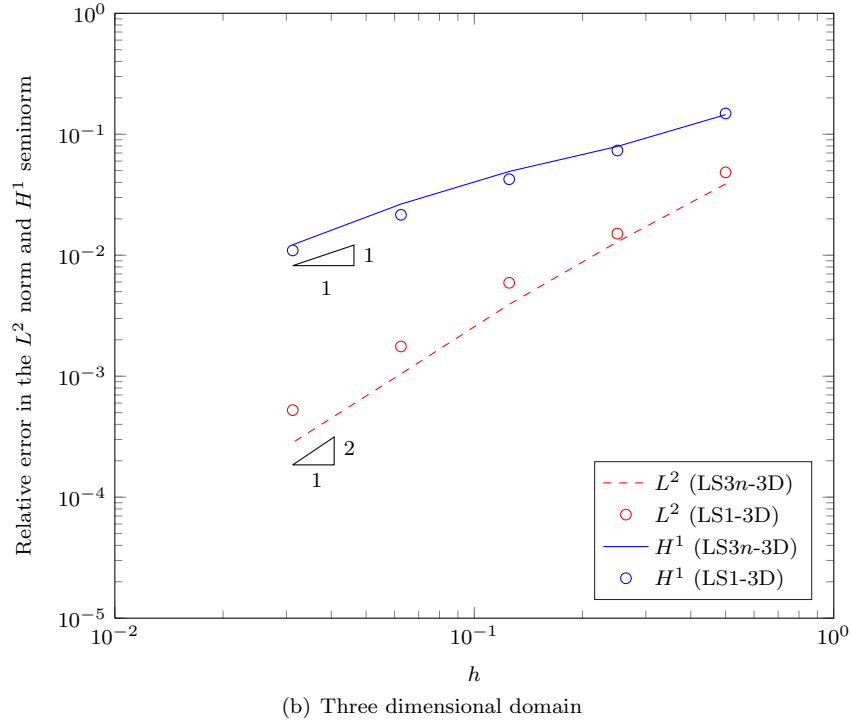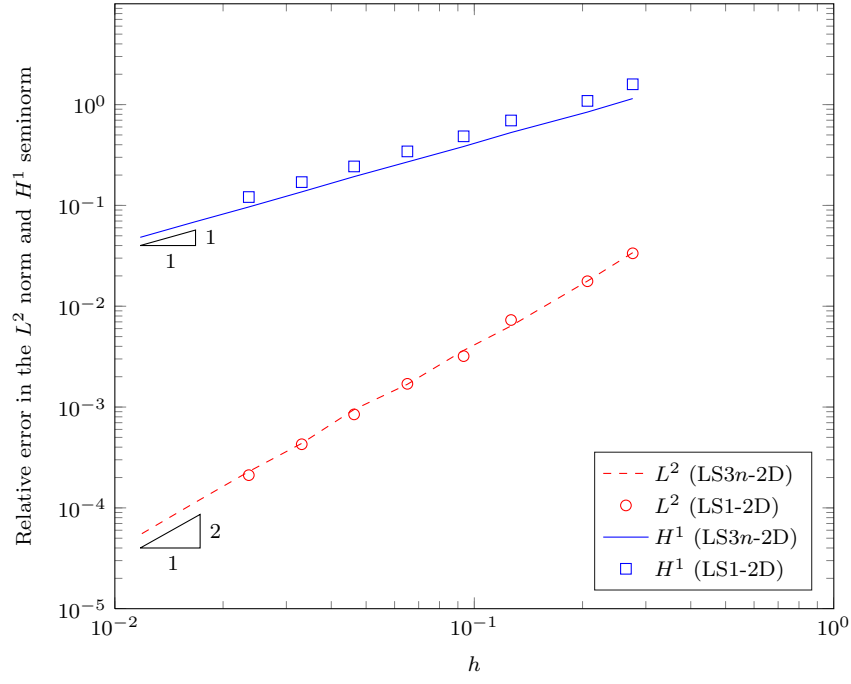
(b) Three dimensional domain

Fig. 5: Convergence results for the quadratic patch test. The domain is discretized with arbitrary polytopes. The new integration scheme delivers optimal convergence rates in both the L^2 norm and H^1 seminorm with fewer integration points per element.

properties are: Young's modulus, $E = 3 \times 10^7$ N/m^2, Poisson's ratio $\nu = 0.25$ and the parabolic shear force is $P = 150$ N. The exact solution for the displacement field is given by:

$$u(x, y) = \frac{Py}{6EI}\left[(9L - 3x)x + (2 + \nu)\left(y^2 - \frac{D^2}{4}\right)\right],$$

$$v(x, y) = -\frac{P}{6EI}\left[3\nu y^2(L - x) + (4 + 5\nu)\frac{D^2 x}{4} + (3L - x)x^2\right]. \tag{31}$$

where $I = D^3/12$ is the second area moment. A state of plane stress is considered. Figure 7 shows few sample polygonal meshes. The numerical convergence of the relative error in the L^2 norm and the H^1 seminorm is shown in Figure 8. It can be seen that the proposed one point integration rule yields optimal convergence rate in both the L^2 norm and the H^1 seminorm. With mesh refinement the solution approaches the analytical solution asymptotically. It is further noted that the proposed integration rule yield similar results when compared to the recently proposed integration rule [1] that employs $3n$ integration point per element, where n is the number of sides of a polygon.
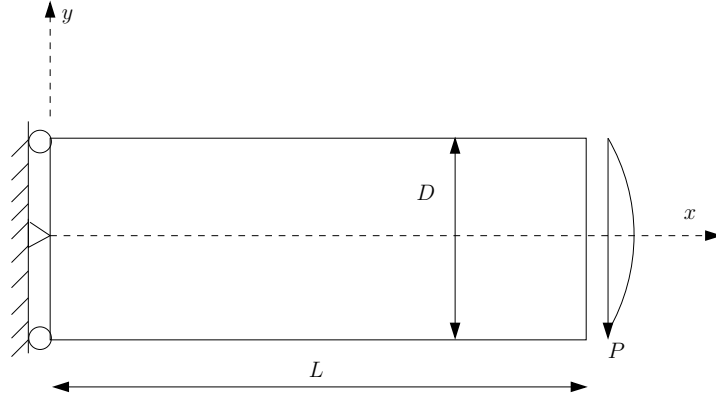

Fig. 6: Geometry and boundary conditions for the two dimensional cantilever beam problem.

4.3 Three dimensional cantilever beam under end torsion

Consider a prismatic cantilever beam with $\Omega : [-1, 1] \times [-1, 1] \times [0, L]$ (see Figure 9 for geometry of the domain) subjected to end torsion. The material is assumed to be homogeneous and isotropic with Youngs' modulus, $E = 1$ N/m^2, Poisson's ratio $\nu = 0.3$ and shear modulus $G = E/(2(1 + \nu))$. Two different loading conditions, viz., end shear load and end torsion, are considered here for which analytical solutions are available in the literature. The accuracy and the convergence properties are studied for random closed-pack Voronoi mesh. Figure 10 shows a few representative random Voronoi meshes employed for this study.

The exact displacement solution for this boundary value is [49]:

$$\begin{aligned}
u_x &= -\beta yz \\
u_y &= \beta xz \\
u_z &= \beta\left[xy + \sum_{n=1}^{\infty} \frac{32a^2(-1)^n}{\pi^3(2n - 1)^3} \sin\left((2n - 1)\frac{\pi x}{2a}\right)\frac{\sinh((2n - 1)\frac{\pi y}{2a})}{\cosh((2n - 1)\frac{\pi y}{2a})}\right]
\end{aligned} \tag{32}$$

where the constant β is proportional to the total torque applied to the beam. The exact Cauchy stress field is given by:

$$\begin{aligned}
\sigma_{xx} &= \sigma_{xy} = \sigma_{yy} = \sigma_{zz} = 0 \\
\sigma_{xz} &= G\beta \sum_{n=1}^{\infty} \frac{16a(-1)^n}{\pi^2(2n - 1)^2} \cos\left((2n - 1)\frac{\pi x}{2a}\right)\frac{\sinh((2n - 1)\frac{\pi y}{2a})}{\cosh((2n - 1)\frac{\pi y}{2a})} \\
\sigma_{yz} &= G\beta\left[2x + \sum_{n=1}^{\infty} \frac{16a(-1)^n}{\pi^2(2n - 1)^2} \sin\left((2n - 1)\frac{\pi x}{2a}\right)\frac{\cosh((2n - 1)\frac{\pi y}{2a})}{\cosh((2n - 1)\frac{\pi y}{2a})}\right]
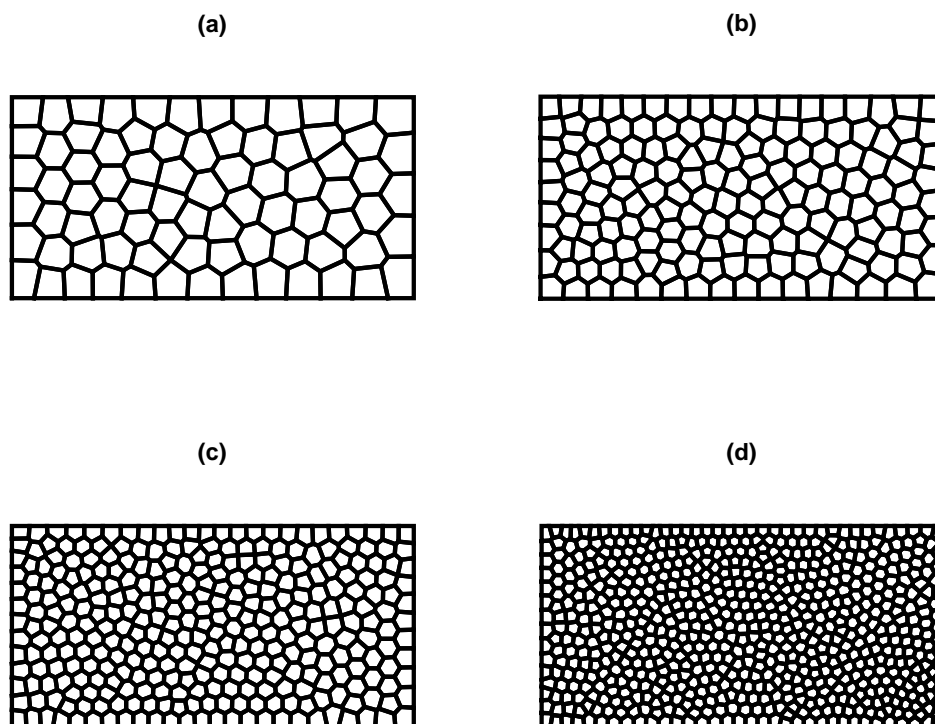\end{aligned} \tag{33}$$

(a)

(b)

(c)

(d)

Fig. 7: Sample meshes for the two dimensional cantilever beam problem containing: (a) 80, (b) 160, (c) 320 and (d) 640 polygons.

The infinite series in Equations (32) - (33) is truncated at $n = 40$. The exact solution for the displacement is prescribed on the surface at $z = L$ and at $z = 0$, surface tractions are applied which are consistent with the exact stress field. The convergence of the proposed technique over arbitrary polyhedron with mesh refinement is studied. The error in the L^2 and the H^1 seminorm is shown in Figure 11 and it can be seen that the proposed approach yields optimal convergence rate. The results from the present approach is compared with linear smoothing technique that employs 4 integration points per tetrahedra.

5 Concluding Remarks

Linearly consistent one point quadrature rule has been proposed to integrate over star convex arbitrary polytopes. The results from the proposed scheme is compared with the linear smoothing scheme. In case of linear smoothing scheme, for example, LS3n-2D/LS3n-3D, the element is sub-divided into triangles or tetrahedra in two and three dimensions. The linear smoothing scheme is then performed over each triangle. This process requires $3n$ integration points per element, where n is the number of sides of the element. In the proposed scheme, no such subdivisions is necessary. Moreover it only requires *one* integration point per element. This significantly reduces the computational effort. The proposed integration rule yields accurate results and converges with optimal rate in bot the L^2 norm and in H^1 seminorm.

References

1. S.P.A.B. A. Francis, A.Ortiz-Bernardin, S. Natarajan, International Journal for Numerical Methods in Engineering **109**(9), 1263 (2017). Nme.5324
2. N. Sukumar, E.A. Malsch, Archives of Computational Methods in Engineering **13**(1), 129 (2006). DOI 10.1007/BF02905933. URL http://dx.doi.org/10.1007/BF02905933
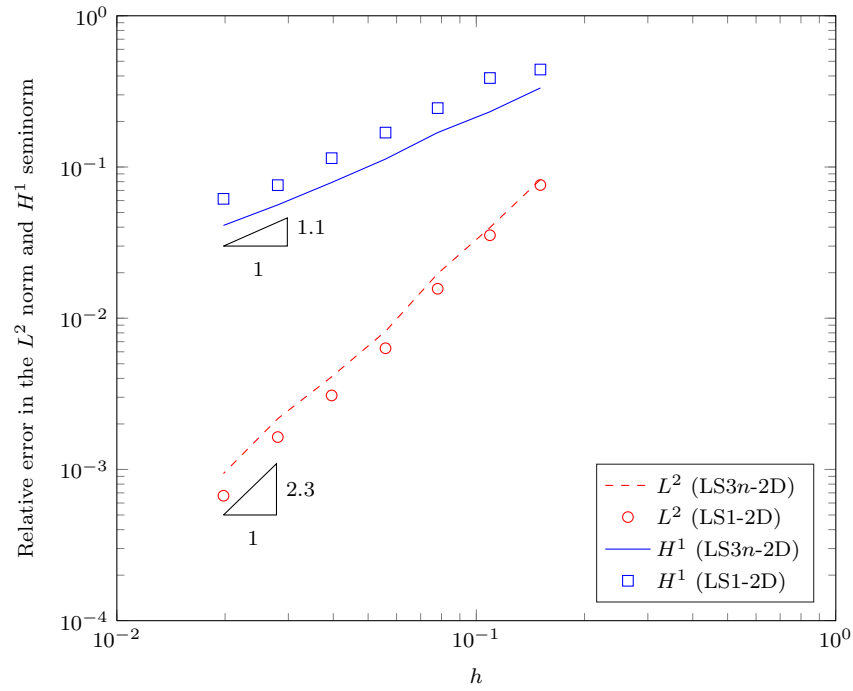
Fig. 8: Convergence of the relative error in the L^2 norm and the H^1 seminorm with mesh refinement for a two-dimensional cantilever beam subjected to end shear. It is inferred that the proposed integration scheme yields optimal convergence rate and accurate results.
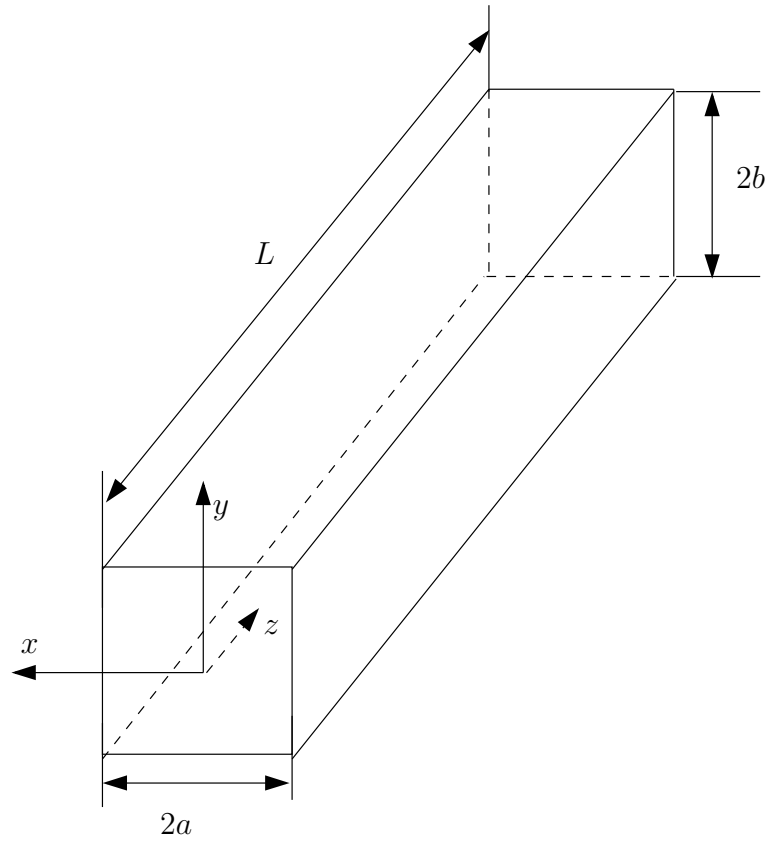

Fig. 9: Cantilever beam: (a) Geometry, length L and rectangular cross-section of width $2a$ and height $2b$. For the present study, the following dimensions are considered: $L = 5$, $a = b = 1$.
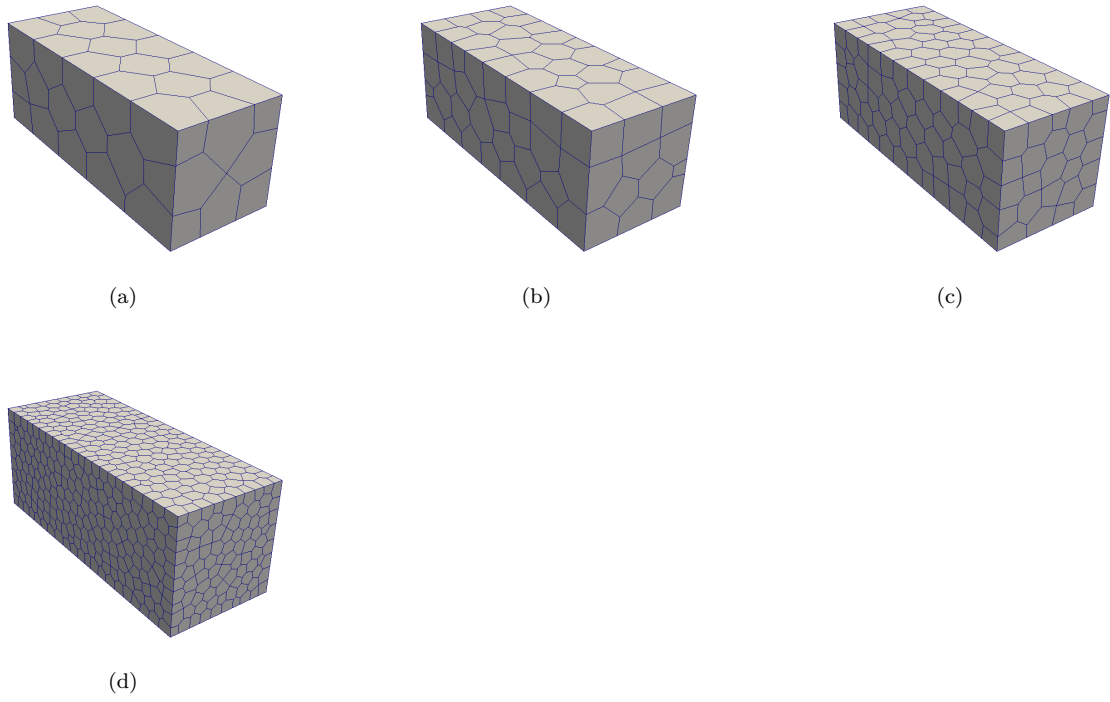
Fig. 10: Sample meshes for the three dimensional cantilever beam problem containing (a) 50, (b) 100, (c) 300 and (d) 2000 polyhedra.
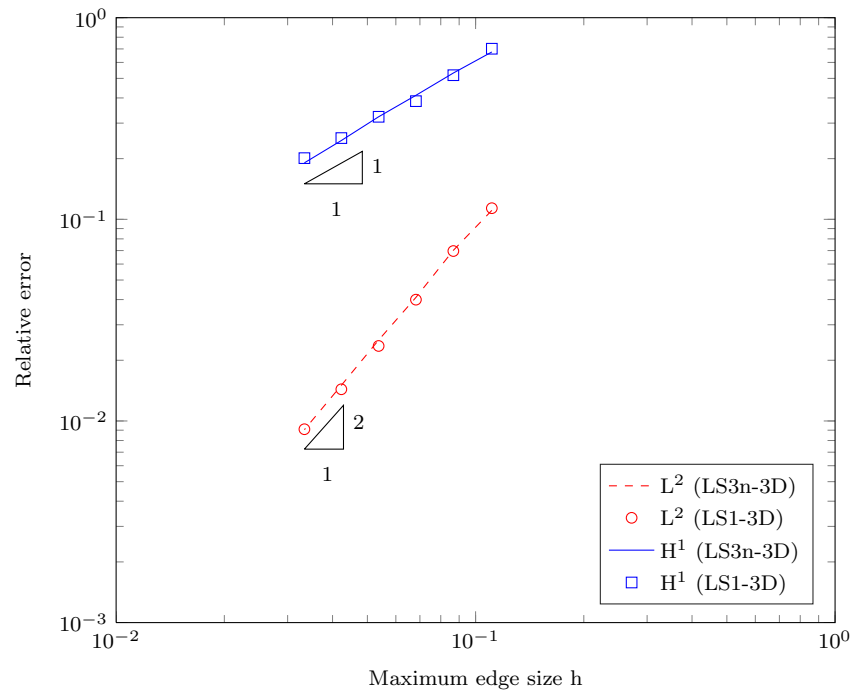

Fig. 11: Convergence of the relative error in the L^2 norm and the H^1 seminorm with mesh refinement for the three-dimensional cantilever beam problem subjected to end torsion. It can be seen that the proposed integration rule yields similar results when compared to linear smoothing scheme. The rate of convergence is also optimal in both the L^2 norm and in the H^1 seminorm.

3. N. Sukumar, International Journal for Numerical Methods in Engineering **61**(12), 2159 (2004)
4. A.G. A. Rand, C. Bajaj, Mathematics of Computation **83**, 2691 (2014)
5. A.P. C. Talischi, G. H. Paulino, I.F.M. Menezes, Struct. Multidisc. Optim. **45**, 309 (2012)
6. P.P. J. Jaskowiec, A. Stankiewicz, Finite Elements in Analysis and Design **120**, 1 (2016)
7. K. Sze, N. Sheng, Finite Elements in Analysis and Design **42**(2), 107 (2005)
8. A.A. K. Jayabal, A. Menzel, S. Srinivasan,
9. S.O.R. Biabanaki, A.R. Khoei, Computational Mechanics **50**(1), 19 (2012)
10. H. Chi, Polygonal finite elements for finite elasticity. Master's thesis, University of Illinois at Urbana-Champaign (2014)
11. G.H.P.I.M. C. Talischi, A. Pereira, M. Carvalho, International Journal for Numerical Methods in Engineering **74**(2), 134 (2014)
12. A.R.K. S.O.R. Biabanaki, P. Wriggers, Computer Methods in Applied Mechanics and Engineering **269**(1), 198 (2014)
13. R.Y. A. R. Khoei, S. Biabanaki, International Journal of Fracture **194**(2), 123 (2015)
14. S.N. Hoang, H.N. Xuan, International Journal for Numerical Methods in Engineering (2016). DOI 10.1002/nme.5448
15. F.B. N. Bellomo, G. Manzini, Mathematical Models and Methods in Applied Sciences **24**(8), 1453 (2014)
16. K. Lipnikov, G. Manzini, Journal of Computational Physics **272**(1), 360 (2014)
17. G.M. V. Gyrya, K. Lipnikov, D. Svyatskiy, Mathematical Models and Methods in Applied Sciences **24**(08), 1621 (2014)
18. L.D.M. L. Beirao da Veiga, F. Brezzi, A. Russo, Mathematical Models and Methods in Applied Sciences **24**(08), 1541 (2014)
19. J. Droniou, Mathematical Models and Methods in Applied Sciences **24**, 1575 (2010)
20. E.H.G. A. Cangiani, P. Houston, Mathematical Models and Methods in Applied Sciences **24**(10), 2009 (2014)
21. A.C.G.M.L.D.M. L Beirao da Veiga, F Brezzi, A. Russo, Mathematical Models and Methods in Applied Sciences **23**, 199 (2013)
22. S.S. P. F. ANTONIETTI, M. BRUGGI, M. VERANI, Mathematics- Numerical Analysis (2016). URL arXlv:1612.08620
23. A.R. G. Manzini, N. Sukumar, Mathematical Models and Methods in Applied Sciences **24**, 1665 (2014)
24. L.B.D. Veiga, G. Manzini, The mimetic finite difference method and the virtual element method for elliptic problems with arbitrary regularity. Tech. Rep. LA-UR-12-22977, Los Alamos National Laboratory (2012)
25. C.T. L. Arun, G.H. Paulino, Computer Methods in Applied Mechanics and Engineering **282**(1), 132 (2013)
26. S.P.A.B. S. Natarajan, E.T. Ooi, International Journal for Numerical Methods in Engineering **104**, 1173 (2015). DOI 10.1002/nme.4965
27. M.S. Floater, Computer Aided Geometric Design **20**(1), 19 (2003)
28. J. Bishop, International Journal for Numerical Methods in Engineering **97**, 1 (2013)
29. N. Sukumar, A. Tabarrei, European Congress on Computational methods in applied sciences and engineering pp. 24–28 (2004)
30. N. Sukumar, International Journal for Numerical Methods in Engineering **61**, 2159 (2004)
31. C.S. E. Ooi, S. Natarajan, International Journal for Numerical Methods in Engineering **108**(9), 1086 (2016)
32. C. Talischi, G.H. Paulino, Mathematical Models and Methods in Applied Sciences **24**(8), 1701 (2014)
33. N. Sukumar, A. Tabarrei, International Journal for Numerical Methods in Engineering **61**, 2045 (2004)
34. S.Y. J. S. Chen, C.T. Wu, Y. You, International Journal for Numerical Methods in Engineering **50**(2), 435 (2001)
35. K.Y.D. G.R. Liu, T.T. Nguyen, Computational Mechanics **39**, 859 (2007)
36. K.Y.D. G. R. Liu, T. T. Nguyen, K.Y. Lam, International Journal for Numerical Methods in Engineering **71**(8), 902 (2007)
37. H.N.X. G. R. Liu, T. N. Thoi, K. Lam, Computers and Structures **87**, 14 (2009)
38. P.K. C. K. Lee, L. A. Mihai, S.P.A. Bordas, (2014). URL http://orbilu.uni.lu/bitstream/10993/14933/1/CKpaper.pdf
39. T.N.T. G. R. Liu, K. Lam, Journal of Sound and Vibration **320**, 1100 (2009)
40. T.N.T. G. R. Liu, K. Lam, Computer Methods in Applied Mechanics and Engineering **197**, 3883 (2008)
41. S.N. S. P. A. Bordas, P. Kerfriden, International Journal for Numerical Methods in Engineering **86**, 637 (2011)
42. I.C. S. Natarajan, E. T. Ooi, C. Song, Finite Elements in Analysis and Design **85**, 101 (2014)
43. H.Z. Q. Duan, X. Li, T. Belytschko, International Journal for Numerical Methods in Engineering **92**(4), 399 (2012)
44. B.W.X.L.H.Z.T.B. Q. Duan, X. Gao, Y. Shao, International Journal for Numerical Methods in Engineering **99**(2), 79 (2014)
45. B.W.X.L. Q. Duan, X. Gao, H. Zhang, **280**(0), 84 (2014)
46. N. Sukumar, Computer Methods in Applied Mechanics and Engineering **263**, 27 (2013)
47. J.S.H. A. Ortiz-Bernardin, C.J. Cyron, **285**, 427 (2015)
48. M.A.P. A. Ortiz-Bernardin, N. Sukumar, **293**, 348 (2015)
49. J. Barber, *Elasticity* (Springer, New York, 2010)